

Highly confined electromagnetic fields in arrays of strongly coupled Ag nanoparticles

L. A. Sweatlock,* S. A. Maier, and H. A. Atwater

Thomas J. Watson Laboratory of Applied Physics, California Institute of Technology, Pasadena, California 91125, USA

J. J. Penninkhof

Center for Nanophotonics, FOM-Institute AMOLF, Kruislaan 407, 1098 SJ Amsterdam, The Netherlands

A. Polman

Thomas J. Watson Laboratory of Applied Physics, California Institute of Technology, Pasadena, California 91125, USA and Center for Nanophotonics, FOM-Institute AMOLF, Kruislaan 407, 1098 SJ Amsterdam, The Netherlands

(Received 1 December 2004; revised manuscript received 16 February 2005; published 10 June 2005)

Linear arrays of very small Ag nanoparticles (diameter ~ 10 nm, spacing 0–4 nm) were fabricated in sodalime glass using an ion irradiation technique. Optical extinction spectroscopy of the arrays reveals a large polarization-dependent splitting of the collective plasmon extinction band. Depending on the preparation condition, a redshift of the longitudinal resonance as large as 1.5 eV is observed. Simulations of the three-dimensional electromagnetic field evolution are used to determine the resonance energy of idealized nanoparticle arrays with different interparticle spacings and array lengths. Using these data, the experimentally observed redshift is attributed to collective plasmon coupling in touching particles and/or in long arrays of strongly coupled particles. The simulations also indicate that for closely coupled nanoparticles (1–2 nm spacing) the electromagnetic field is concentrated in nanoscale regions (10 dB radius: 3 nm) between the particles, with a 5000-fold local field intensity enhancement. In arrays of 1-nm-spaced particles the dipolar particle interaction extends to over 10 particles, while for larger spacing the interaction length decreases. Spatial images of the local field distribution in 12-particle arrays of touching particles reveal a particlelike coupled mode with a resonance at 1.8 eV and a wirelike mode at 0.4 eV.

DOI: 10.1103/PhysRevB.71.235408

PACS number(s): 73.20.Mf, 78.67.Bf, 42.79.–e, 71.45.Gm

I. INTRODUCTION

In recent years, significant progress has been made towards reducing the size of optical devices. This trend towards miniaturization is driven by the increase in system functionality and reduction in power dissipation that may be achieved when highly integrated photonic networks replace today's discrete devices and stand-alone modules. Another important motivation is a vision of an architecture in which photonic circuits integrate seamlessly into large-scale electronic systems. This requires waveguides that bridge the gap in size between conventional micron-scale integrated photonics and nanoscale electronics. Additionally, nanostructured materials often possess strong nonlinear properties that can be exploited in the development of novel active devices, since the confinement of light to small volumes can lead to nonlinear optical effects even with modest input power.

In purely dielectric materials, the optical diffraction limit places a lower bound on the transverse dimension of waveguide modes at about $\lambda_0/2n$ —i.e., several hundreds of nanometers for visible light.^{1,2} Plasmonic waveguides, on the other hand, employ the localization of electromagnetic fields near metal surfaces to confine and guide light in regions much smaller than the free-space wavelength and can effectively overcome the diffraction limit.

In plasmonic systems there is generally a trade-off between the size of the electromagnetic mode and loss in the metallic structures. With this design principle in mind there are several choices for plasmonic waveguiding technologies which may prove useful for various applications. For ex-

ample, thin metal stripes support long-range surface plasmon polaritons with an attenuation length as long as millimeters, but lack subwavelength mode confinement.^{3–6} Another geometry is metallic nanowires, which indeed can provide lateral confinement of the mode below the optical diffraction limit. Nanowires have larger attenuation than planar films, but light transport over a distance of several microns has been demonstrated.⁷ Finally, metal nanoparticles are used to achieve three-dimensional, (3D) subwavelength confinement of optical-frequency electromagnetic fields in resonant “particle plasmon” modes.^{8–10} Nanoparticles provide highly enhanced local fields which are promising for molecular sensors^{11–14} or miniature nonlinear optical elements,^{15–19} and arrays of these particles can act as waveguides over modest distances.²⁰ Indeed, linear chains of metal nanoparticles have been shown to support coherent energy propagation over a distance of hundreds of nanometers²¹ with a group velocity around two-tenths the speed of light in vacuum.²² The minimum length scales in fabricated structures were determined by the resolution of electron beam lithography, with particle diameters of $30 \times 30 \times 90$ nm³ and interparticle spacings of 50 nm.

In this paper, we investigate the mode confinement and plasmon coupling in nanostructures with even smaller length scales, composed of linear chain arrays of Ag nanoparticles with diameters in the 10 nm range and interparticle spacing as small as several nanometers. This work is inspired by our recent experimental results in which linear Ag nanoparticle chain arrays with such small length scales are formed in silica glass by ion irradiation.²³ Other methods for generating

very small ordered metal structures include pulsed-laser irradiation²⁴ and biologically templated assembly.²⁵

We first present experimental optical extinction spectroscopy data that show evidence for strong plasmon coupling in ion-beam-synthesized Ag nanoparticle chain arrays. We compare experimental extinction data with full-field 3D electromagnetic simulations for arrays with various chain lengths and particle spacings. The simulations corroborate the experimental data and reveal large local-field enhancements in arrays of strongly coupled nanoparticles.

II. NANOPARTICLE ARRAY FABRICATION

Linear nanoparticle arrays in glass are formed by use of a high-energy ion irradiation technique as follows.²³ First, ionic Ag is introduced into sodalime silicate glass (BK7) by immersion in a melt of AgNO₃, 10% by mass, in NaNO₃ at 350 °C for 10 min. Silver displaces the constituent sodium via an ion exchange interaction, resulting in a Ag content of ~6 at. % near the surface. Next the sample is irradiated with 1-MeV Xe ions to a fluence of 1×10^{16} cm⁻² at normal incidence to induce the nucleation and growth of Ag nanoparticles. The typical particle diameter is in the range of 5–15 nm, and the particles preferentially form in a ~80-nm-thick near-surface region of the silica glass.²⁶ Finally, the sample is irradiated with 30-MeV Si ions at an angle of 60° with respect to the surface normal while cryogenically cooled to 77 K.

Figure 1 shows a plan-view transmission electron microscopy (TEM) image on a sample irradiated with 2×10^{14} Si/cm². A polydisperse Ag particle size distribution is found, with a typical diameter of 10 nm and an upper bound of about 20 nm diameter. The majority of Ag particles appear to have been incorporated into quasilinear chain arrays, aligned along the ion beam direction. This observation is confirmed by spatial fast Fourier transform of the image, inset in Fig. 1(a). The redistribution of Ag is ascribed to the effect of the thermal spike caused by silicon ions' electronic energy loss.²⁷ Figure 1(b) shows a magnified view of the particle arrays. While in these plan-view images it is not possible to separately identify individual arrays, as they overlap in the image, we estimate a typical array length of up to ten particles, with particles either touching or very closely spaced.

III. OPTICAL ABSORPTION SPECTROSCOPY

The inset to Fig. 2 shows optical extinction spectra taken under normal incidence of a sample before (“control”) and after irradiation with 2×10^{14} cm⁻² 30 MeV Si. Data were derived from optical transmission spectra measured using a spectroscopic ellipsometer with the incident beam perpendicular to the sample surface. The wavelength was scanned from 300 nm to 1100 nm in 5-nm steps. Before irradiation, an extinction peak is observed at an energy of 3.0 eV (free-space wavelength 410 nm), corresponding to the surface plasmon dipole excitation of isolated small Ag nanoparticles in a sodalime glass matrix (refractive index $n=1.60$). After irradiation, two distinct spectra are observed for incident

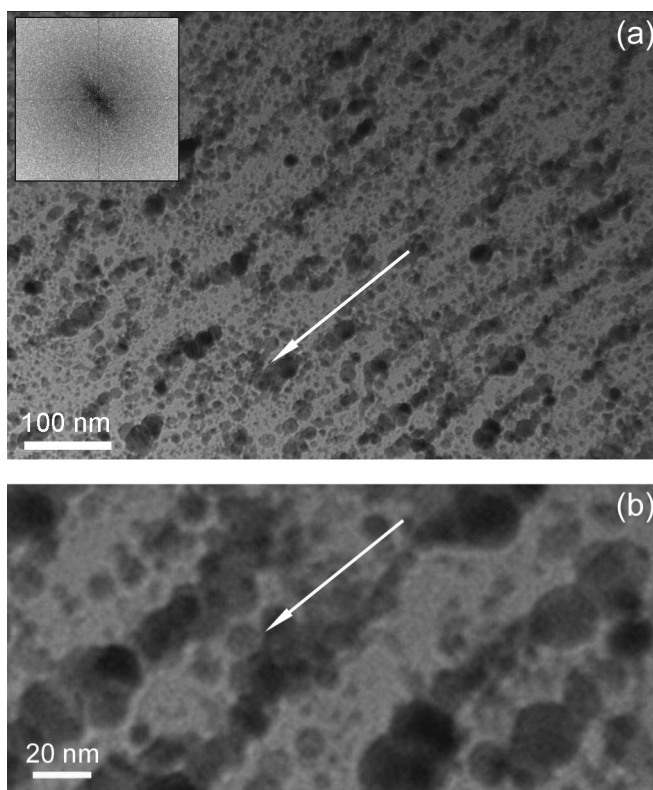


FIG. 1. (a), (b) Plan-view TEM images of Ag nanoparticles in sodalime glass after 30-MeV Si-ion irradiation at two different magnifications. Nanoparticle arrays are observed along the ion beam direction (indicated by arrows). The inset in (a) shows a spatial Fourier transform image of the micrograph confirming this anisotropy. The typical particle diameter in the micrographs is 10 nm, albeit with significant size polydispersity. Touching or closely spaced particles are observed, in arrays with a length of up to ~10 particles.

light polarized either parallel or perpendicular to the ion beam incidence direction projected into the sample surface plane. The splitting of plasmon extinction bands can be explained by “collective particle plasmon” resonances which result from electromagnetic coupling between neighboring particles in linear arrays.^{28,29} When incident light is polarized transverse to the array axis, repulsion between like surface charges on neighboring particles increases the energy required to drive a resonant oscillation and therefore results in a spectral blueshift. Conversely, attraction between nearby unlike surface charges under longitudinally polarized incident light will result in an extinction redshift.

The main panel of Fig. 2 shows the peak energy of the transverse (open circles) and longitudinal (solid) mode extinction spectra as a function of Si ion fluence up to 3×10^{15} cm⁻². The transverse branch shows a modest blueshift that saturates at 3.2 eV (390 nm) while the longitudinal absorption peak can be tuned over a wide range, from 3.0 eV (410 nm) to 1.5 eV (830 nm), into the near infrared.

The longitudinal resonance redshift of over 1.5 eV is much greater than that previously recorded in chains of noble-metal particles with relatively large diameter and spacing, for which a redshift of 100 meV is observed.^{21,22,30} The

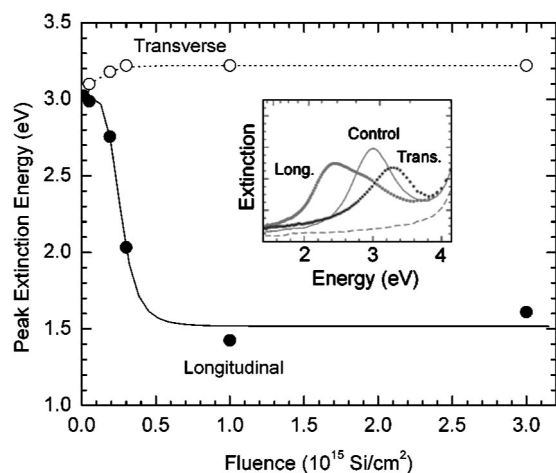


FIG. 2. Measured optical extinction resonance peak energy for silver nanoparticle arrays in glass as a function of 30 MeV Si fluence. The polarization of the incident light is transverse (open circles) or longitudinal (solid) to the projection of the ion beam direction into the normal plane. Inset: typical extinction spectra for both polarizations in a sample before irradiation (“control”) and after irradiation with 2×10^{14} 30 MeV Si cm^{-2} .

1.5-eV shift is attributed to the very strong particle coupling in the present arrays. The ability to tune the resonance frequency into the near infrared is clearly valuable, as it enables applications in the important telecommunications band around $1.5 \mu\text{m}$. Also, the strong interparticle coupling implies a large enhancement of electromagnetic fields³¹ in the interparticle gaps, as will be discussed further on. In the context of nanoparticle waveguides, the extraordinarily large splitting of the plasmon bands indicates a large bandwidth and high group velocity for transport.^{32,33} However, very strongly coupled nanoparticles are suitable for waveguiding only over short distances, as significant spatial overlap of the mode with the metal particle leads to severe damping.³⁴

IV. FINITE INTEGRATION SIMULATION PROCEDURE

The influence of geometrical parameters on the collective plasmon resonance of linear chains of Ag nanospheres is studied by three-dimensional full-field electromagnetic simulations which employ finite-element integration techniques to solve Maxwell’s equations.³⁵ We keep the particle size constant at 10 nm diameter and assume that the particles are spaced evenly along a line with perfect axial symmetry. Particle spacing was varied from 0 nm (touching particles) to 4 nm. The optical constants of Ag are modeled with a Drude model:

$$\epsilon(\omega) = 5.45 - 0.73 \frac{\omega_p^2}{\omega^2 - i\omega\gamma}, \quad (1)$$

with $\omega_p = 1.72 \times 10^{16} \text{ rad s}^{-1}$ and $\gamma = 8.35 \times 10^{13} \text{ s}^{-1}$, which provides a good fit to tabulated experimental data³⁶ throughout the visible and infrared. The index of the surrounding glass matrix is set to $n = 1.60$. The simulation volume is a

rectangular solid which extends at least 100 nm beyond the nanoparticle surfaces in all directions. The mesh is linearly graded with a 10:1 ultimate ratio; i.e., if the grid cells in the immediate vicinity of the particles are $\sim 0.25 \text{ nm}$ on each side, those on the outer boundary of the simulation volume are $\sim 2.5 \text{ nm}$ on each side. Technical limitations constrain the mesh size under these conditions to about 2×10^6 total grid cells. In all simulations the incident light is polarized longitudinally relative to the array. We focus on the longitudinal plasmon resonance because the optical response has a strong functional dependence on geometrical parameters and because the extraordinary tunability of the longitudinal resonance may be of interest for a variety of applications.

A two-step process is used to find the collective particle-plasmon resonant mode and its frequency for each array. First, the simulation volume is illuminated by a propagating plane wave with an off-resonance frequency that allows the particle chain to absorb energy. Second, the incident field is switched off and the electric field amplitude is observed in the time domain as any particle modes excited by the incident plane wave resonantly decay or “ringdown.” The data presented below are all monitored at nanoparticle centers, but in general the time response of the electric field in interparticle gaps and other points of lower symmetry are also observed to provide additional information about the mode structure. A fast Fourier transform (FFT) of these data gives the spectral response that enables the resonant frequencies to be identified. Since the absorption and ringdown are resonant phenomena, the frequency at which the peak FFT response occurs is directly comparable to the frequency of maximum extinction in an optical spectrum. Once the spectrum was outlined in this way, on-resonance excitation was used to excite individual modes to examine the corresponding spatial distribution of the field intensity. Such distributions can be used to discriminate between spectral features which correspond to the collective dipole excitation and other physical resonances or, in some cases, unphysical artifacts of the simulation or frequency domain transform which can be eliminated once identified. In some cases small “hot spots” were observed in the intensity maps, which occurred at slight faceted corners of the rendered nanospheres. By varying the grid size and geometry these were identified as artifacts of the simulation. When the grid cell linear dimensions were reduced to 0.25 nm in the immediate vicinity of the metal nanoparticles, these hot-spot artifacts had a negligible effect on the overall field distribution. This requisite fine mesh density has the indirect effect of constraining the maximum simulation size to linear arrays of about 12 nanoparticles.

Figure 3(a) shows peak-normalized Fourier transform amplitude spectra of particle ringdown for four-particle chains of 10-nm-diam Ag particles, with interparticle spacings of 1 nm, 2 nm, and 4 nm, and for an isolated particle. We verified that the peak frequency value is robust against small changes to the mesh cell density, sphere smoothness, or other minor variations in simulation procedure. In contrast, the apparent linewidth and spectral shape of the resonance were found to be somewhat dependent on arbitrary factors such as the total ringdown time and the absorption cross section of the structure at the off-resonance excitation frequency. The Fourier transform spectra often also contain several peaks

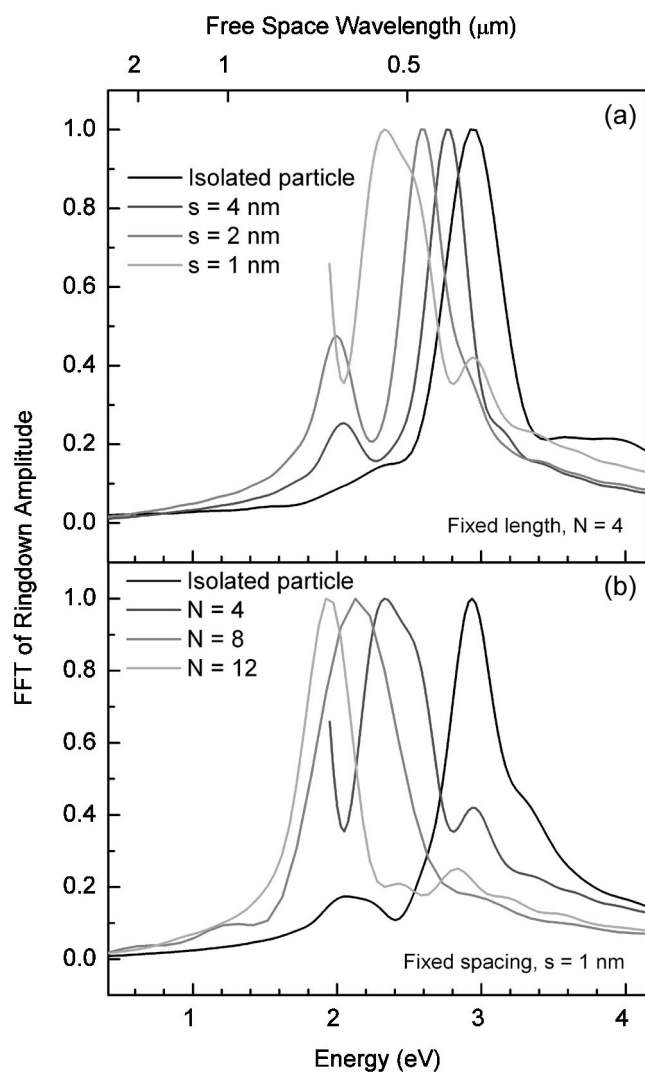


FIG. 3. Simulated longitudinal extinction spectra for linear arrays of 10-nm-diam Ag particles in glass. (a) Array of four particles spaced by 1, 2, or 4 nm. (b) Array of 4, 8, or 12 particles with interparticle spacing fixed at 1 nm. A reference spectrum for a single Ag particle is also shown in each panel. Each spectrum is normalized to the height of the strongest extinction peak, which we identify as the collective dipole resonance.

with normalized amplitude less than one. Investigation of spatial energy density profiles using selective-frequency excitation revealed that low-energy secondary peaks [e.g., around 2 eV in Fig. 3(a)] correspond to artifact modes particular to the 3D polygonal representation of the nanoparticle. The weak features observed in the spectra of Fig. 3 at energies slightly greater than that of the primary peak likely correspond to real multipolar nanoparticle resonances. Selective-frequency excitation simulation of these features proves impossible due to the low scattering strength of these resonances and spectral proximity to the primary peak. The primary peak, however, was found to correspond to the dipole excitation in all cases. From the above analysis we conclude that the peak energy of the Fourier transform spectra is a good metric for the dipole resonance energy and can thus be compared with experimental peak extinction energies.

V. RESULTS AND DISCUSSION

The resonance peak for isolated particles in Fig. 3(a) occurs at 2.93 eV (free-space wavelength 424 nm), in good agreement with the experimental data (Fig. 2), indicating that the initially prepared Xe-irradiated sample (i.e., without ordered nanoparticle arrays) consists of uncoupled nanoparticles. This is consistent with earlier work showing that under these Xe irradiation conditions about 33% of the incorporated Ag is agglomerated in nanoparticles with a mean diameter of 5–10 nm, while the remaining 67% remains embedded in the glass network as Ag ions. The corresponding interparticle distance is about three particle diameters, too large for significant interparticle coupling.^{26,37}

Figure 3(a) also shows that a decrease in particle spacing in the four-particle array increases the interparticle coupling, leading to an increased resonance redshift. At 1 nm spacing the simulated resonance occurs at 2.35 eV (528 nm). Figure 3(b) shows the effect of total chain length on simulated spectral response of Ag nanoparticle chains with the interparticle spacing fixed at 1 nm. Data are shown for arrays with a total length of 12, 8, 4, and 1 particle(s). As can be seen, increasing the chain length causes a larger shift towards lower frequencies, implying that the particle interaction extends beyond the first nearest neighbor. In the 12-particle chain the observed frequency is 1.92 eV (647 nm), a difference as large as 1.0 eV compared to the single-particle plasmon resonance. We expect that the effect of increasing chain length will saturate in chains of not more than 20 particles, based on Quinten and Kreibig's numerical calculations for Ag particles in air.²⁸ In less strongly coupled chains, with 2 nm or 4 nm spacing, we found that extending the overall length of the chain beyond four particles did not lead to a further shift in resonance frequency. This result is consistent with our earlier work,³⁴ in which it was reported that in chains of widely spaced and therefore relatively weakly coupled Au particles, the resonance frequency was not a strong function of array length.

Figure 4 shows the spatial images of the peak instantaneous electric field intensity (i.e., E^2) at steady state for arrays of four 10-nm-diam particles, excited on resonance. Data are shown for interparticle spacings of (a) 4 nm, (b) 2 nm, or (c) 1 nm. The background level is normalized to the maximum instantaneous square amplitude of the incident plane wave. Note that this normalization level is different than the plane-wave background at the same instant in time as the field profile snapshot, since there is a phase lag between the amplitude peaks in the driving wave and in the resonant response. Each contour line represents an intensity difference by a factor 1.8 (four lines correspond to one order of magnitude). The maximum local field is observed in the dielectric gap between the two metal particles at the midpoint of the array. The factor by which the field intensity at the array midpoint exceeds the background level is ~ 80 in the weakly coupled array, Fig. 4(a), and ~ 5000 in the more strongly coupled array (c). For comparison, the maximum field intensity enhancement near an isolated nanoparticle driven resonantly is typically 30. The giant 5000-fold intensity enhancement is consistent with previous reports of 10^6 – 10^8 -fold enhancement of the effective Raman scattering cross section

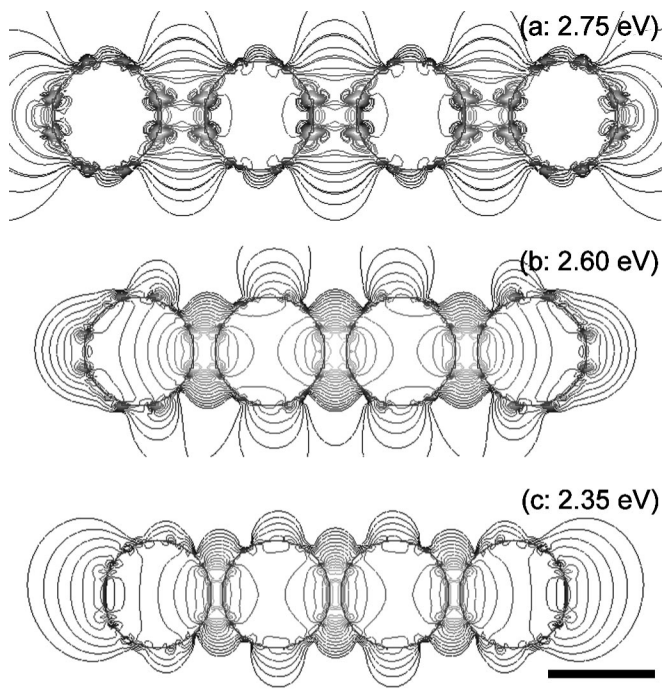


FIG. 4. Two-dimensional spatial images of the electric field intensity in a plane through the particle centers of four Ag nanospheres with interparticle spacing of (a) 4 nm, (b) 2 nm, and (c) 1 nm at resonant excitation. The background is normalized to maximum instantaneous intensity of the incident plane wave. Each contour line represents an intensity difference by a factor of 1.8 (four lines represent one order of magnitude).

near metallic nanostructures, given the fact that Raman scattering is quadratic in field intensity.^{11,12}

Figure 5 shows the field intensity along a line normal to the particle axis through the interparticle gap at the midpoint of a four-particle array. The field confinement is most pro-

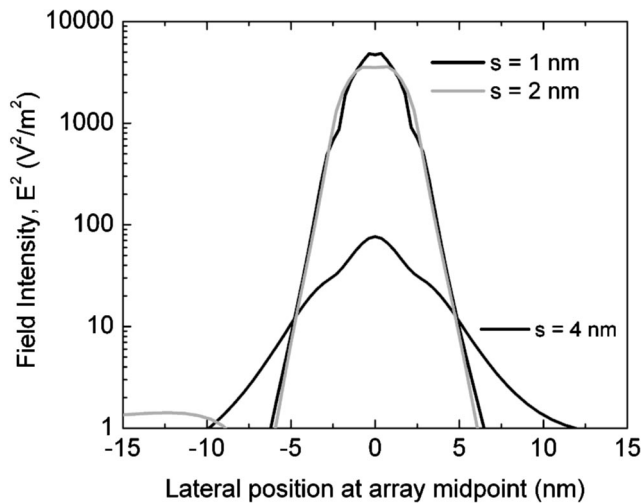


FIG. 5. Electric field intensity on a line through the dielectric gap at the midpoint of an array of four Ag nanospheres with interparticle spacing of (a) 4 nm, (b) 2 nm, and (c) 1 nm at resonant excitation. Maximum instantaneous intensity of the incident plane wave is $1 \text{ V}^2 \text{ m}^{-2}$.

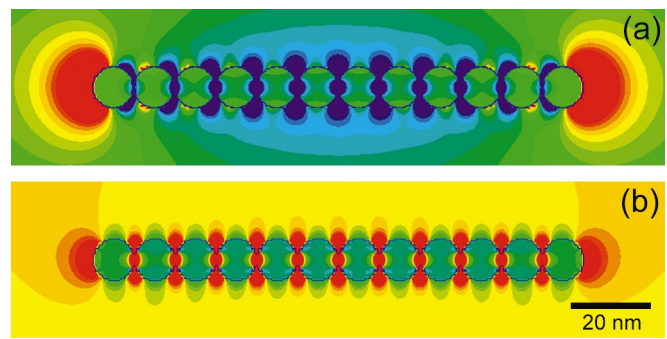


FIG. 6. (Color) Distribution of the longitudinal component of the electric field (E_x) in the vicinity of an array of 12 Ag particles with 10 nm diameter, illustrating two distinct modes. In panel (a), an antennalike mode resembling that of a single elongated wire is excited resonantly at 0.35 eV; in panel (b), a coupled-particle-like mode resembling that of a chain of independent particles is excited resonantly at 1.65 eV. The slight axial asymmetry of the field distribution is caused by superposition of the resonant mode with the exciting plane wave.

nounced for the array with the smallest spacings, 1 nm and 2 nm, where the lateral distance (from the array axis) at which the field diminishes by 10 dB is 3 nm; it vanishes by 30 dB in less than 6 nm. Given that the resonant excitation wavelength for this mode in bulk glass is 330 nm, this clearly demonstrates the giant field enhancement and localization in these closely spaced nanoparticle arrays. Figure 5 also shows that for 4 nm spacing the field is less concentrated, with a 10 dB decay distance of 5.5 nm and peak field intensity nearly 100-fold lower than for the 1-nm-spaced array. This demonstrates that true nanoscale engineering is required to advantage of these high-field-concentration effects. Indeed, the ion-irradiation-induced nanoparticles arrays in Fig. 1 are an example of that.

In TEM images such as Fig. 1 we observe a strong possibility that in some arrays the interparticle separation has been reduced to the point that the nanoparticles just touch their neighbors. We refer to these arrays as having “0 nm interparticle spacing.” In simulations the touching spheres are defined to overlap each other by about 0.25 nm (one grid cell depth) and therefore share a circular boundary surface with a radius of about 1 nm. In this case two distinct longitudinal modes are found in the spectrum. For an array length of 12 particles these occurred at 0.35 eV (free-space wavelength 3500 nm) and 1.65 eV (750 nm). As described in Sec. IV, we selectively excite and study the spatial distribution of the electric field for the two cases. In this case, however, the additional low-energy peak is not an edge or corner artifact but has real physical significance. This is demonstrated in Fig. 6, which shows the longitudinal component (E_x) of the electric field in a system which consists of a linear array of 12 touching Ag spheres excited at the two resonance frequencies. Areas colored red have positive field amplitude, while areas colored blue have negative field amplitude. In a snapshot of the chain driven by a longitudinally polarized plane wave at 0.35 eV [panel (a)], regions of positive E_x are observed at either end, with negative E_x throughout the body of the array. This electric field pattern indicates that positive

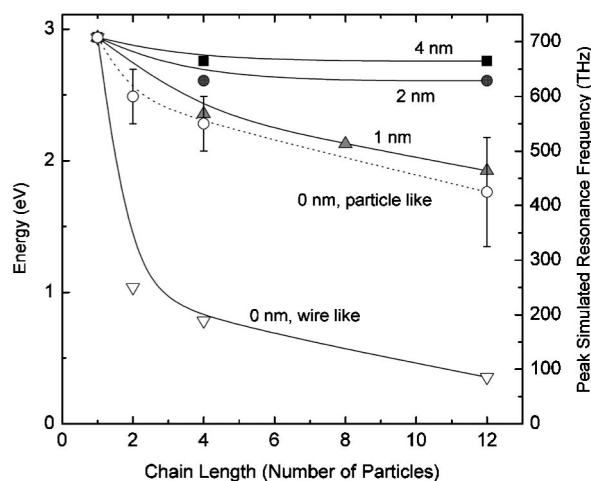


FIG. 7. Simulated longitudinal collective resonance frequency for linear arrays of various overall length, ranging from 1 to 12 Ag particles each 10 nm in diameter. Series represent interparticle spacings from 0 to 4 nm. In the case of zero nanometer spacing, the frequencies of both coupled-nanoparticle-like and -wire-like modes are plotted.

surface charge is concentrated on the rightmost particle and negative charge on the leftmost particle. The mode is typical of a single-wire antenna and requires surface charge to flow from particle to particle along the entire length of the array. Alternatively, when the same structure is driven at 1.65 eV [panel (b)] the coupled-dipole resonance is selectively excited. The field diagram alternates from positive in each dielectric gap to negative inside each particle. This indicates an alternating surface-charge distribution in which each individual particle is polarized but electrically neutral. Thus, in the touching-particle configuration, the system can support two kinds of longitudinal resonance: the particles can still act as individual coupled dipoles or, instead, as a single-continuous-wire antenna.

Although particle like and wirelike modes of touching-particle chains have strongly shifted peak resonance frequencies, we found that they do not in general exhibit an extremely high degree of local-field amplification. The lack of a dielectric gap means that the interparticle interaction is only weakly capacitive in nature, and therefore only a small magnitude of opposing surface charge builds up on neighboring particles. However, a contrary influence also comes into play. The sharp “crevice” formed between two intersecting spheres may contribute to shape-induced enhancement to the local fields. For the specific geometric configuration and material properties input to our simulation, we found the former effect to dominate. Various aspects of coupled modes in nanoparticle dimers, including the touching-particle case, are discussed in Refs. 38–40.

Figure 7 shows a compilation of longitudinal resonance energies for linear arrays of 10-nm-diam Ag particles, plotted as a function of chain length. The data series represent interparticle spacings of 4, 2, 1, or 0 nm. In the case of zero nanometer spacing, the energies of “particlelike” and “wirelike” modes are plotted separately. The particlelike resonances are relatively weak, leading to some uncertainty in

their position, as indicated by error bars on that series. The figure shows that for 12-particle array length the resonance of the most strongly coupled arrays (0 or 1 nm spacing) shifts by about 1 eV to a peak resonance energy around 2 eV. More weakly coupled chains saturate at peak energies above ~ 2.5 eV.

We now compare these data with the experimental particle distributions and resonance energy measurements in Figs. 1 and 2. Although the nanoparticle distributions are quite inhomogeneous, indeed, touching and nearly touching particles are observed in the TEM, which according to our simulations lead to large plasmon shifts. The decrease in plasmon energy with increasing fluence (Fig. 2) can be attributed to either (or both) a gradual growth in particle array length or a decrease in interparticle spacing. The experimentally observed peak resonance for high-fluence irradiation in Fig. 2 is 1.5 eV. The resulting resonance energy is thus lower than the lowest coupled-particle mode energy calculated in Fig. 7 (1.8 eV). This may indicate that long chains ($N > 12$ particles) form at large fluence. Alternatively, wirelike modes in small chains could be dominating as the interparticle spacing approaches zero. Further investigation of the relative interaction cross section for the wire and particle modes would be necessary to support this hypothesis.

For applications of field enhancements at the important telecommunication wavelength of $1.5 \mu\text{m}$ (0.8 eV), very strongly coupled arrays of nanoparticles are required. Comparing our data with those our results from arrays of larger particles²² and with previous results in the literature²⁸ it appears that it is the combination of particle center-to-center spacing and diameter, rather than interparticle spacing alone, that is a key parameter determining the coupling strength. Finally, we note possible applications of the wirelike mode in the THz-frequency domain, in particular for very long array lengths.

VI. CONCLUSION

Linear arrays of very small Ag particles in glass, made using ion irradiation, show a strong anisotropy in optical extinction spectra, which is attributed to strong coupling between the particle plasmons. Full-field simulations of the electromagnetic field distribution on arrays of closely spaced Ag nanoparticle arrays show that coupling between the plasmonic particle modes leads to a reduction in the longitudinal resonance energy. In weakly coupled arrays, in which 10-nm particles are separated by 2- or 4-nm interparticle gaps, the resonance shift is less than 0.4 eV. For the “strongly coupled” case of 1 nm spacing or touching particles, a shift larger than 1.0 eV is observed. In those arrays the longitudinal plasmon resonance energy decreases with the total chain length up to at least ten particles. In particle arrays with 1 nm spacing, the simulations indicate a giant 5000-fold enhancement in field intensity between the particles. The resonant electric field is concentrated in extremely small regions with a radial dimension of 3 nm (at the 10-dB point). By comparing the simulated data with the experimental optical

data it is concluded that plasmon coupling behavior in the experimental samples is dominated by short arrays of touching particles and/or long arrays of strongly coupled particles. Due to the great utility of wavelength tunability and local-field enhancement for applications such as nonlinear optics and sensing of small volumes, nanosized ordered or quasior-dered ensembles of very closely spaced metal particles serve as an ideal platform for active device regions in integrated plasmonic networks. Innovative nanoscale engineering and fabrication (such as the ion irradiation technique used here) are required to synthesize particle arrays with these interesting properties.

ACKNOWLEDGMENTS

Bart Kooi (Groningen University) is acknowledged for TEM and Arjen Vredenberg (Utrecht University) for assistance with MeV ion irradiation. Kobus Kuipers (FOM-Institute AMOLF) is gratefully acknowledged for stimulating discussions and advice. David Sheets is acknowledged for scripting simulation macro files. This work was sponsored by G. Pomrenke of the Air Force Office of Scientific Research. The Dutch part of this work is part of the research program of FOM, which is financially supported by NWO.

*Electronic address: lukes@caltech.edu

- ¹R. W. Ditchburn, *Light* (Dover, New York, 1961).
- ²B. E. Saleh and M. C. Teich, *Fundamentals of Photonics* (Wiley, New York, 1991).
- ³D. Sarid, *Phys. Rev. Lett.* **47**, 1927 (1981); A. E. Craig, G. A. Oldon, and D. Sarid, *Opt. Lett.* **8**, 380 (1983).
- ⁴P. Berini, *Phys. Rev. B* **61**, 10484 (2000); **63**, 125417 (2001).
- ⁵T. Nikolajsen, K. Leosson, I. Salakhutdinov, and S. I. Bozhevolnyi, *Appl. Phys. Lett.* **82**, 668 (2003).
- ⁶R. Charbonneau, P. Berini, E. Berolo, and E. Lisicka-Shrzek, *Opt. Lett.* **25**, 844 (2000).
- ⁷J. R. Krenn, B. Lamprecht, H. Ditlbacher, G. Schider, M. Salerno, A. Leitner, and F. R. Aussenegg, *Europhys. Lett.* **60**, 663 (2002).
- ⁸G. Mie, *Ann. Phys.* **25**, 377 (1908).
- ⁹C. F. Bohren and D. R. Huffman, *Absorption and Scattering of Light by Small Particles* (Wiley, New York, 1983).
- ¹⁰U. Kreibig and M. Vollmer, *Optical Properties of Metal Clusters* (Springer-Verlag, Berlin, 1994).
- ¹¹F. J. García-Vidal and J. B. Pendry, *Phys. Rev. Lett.* **77**, 1163 (1996).
- ¹²H. Xu, J. Aizpurua, M. Käll, and P. Apell, *Phys. Rev. E* **62**, 4318 (2000).
- ¹³A. D. McFarland and R. P. Van Duyne, *Nano Lett.* **3**, 1057 (2003).
- ¹⁴D. A. Genov, A. K. Sarychev, V. M. Shalaev, and A. Wei, *Nano Lett.* **4**, 153 (2004).
- ¹⁵F. Hache, D. Ricard, and C. Flytzanis, *J. Opt. Soc. Am. B* **3**, 1647 (1986).
- ¹⁶Y. Hamanaka, K. Fukata, A. Nakamura, L. M. Liz-Marzán, and P. Mulvaney, *Appl. Phys. Lett.* **84**, 4938 (2004).
- ¹⁷R. J. Gehr and R. W. Boyd, *Chem. Mater.* **8**, 1807 (1996).
- ¹⁸Y. Shen and P. N. Prasad, *Appl. Phys. B: Lasers Opt.* **74**, 641 (2002).
- ¹⁹D. Prot, D. B. Stout, J. Lafait, N. Pinçon, B. Palpant, and S. Debrus, *J. Opt. A, Pure Appl. Opt.* **4**, S99 (2002).
- ²⁰M. Quinten, A. Leitner, J. R. Krenn, and F. R. Aussenegg, *Opt. Lett.* **23**, 1331 (1998).
- ²¹S. A. Maier, P. G. Kik, H. A. Atwater, S. Meltzer, E. Harel, B. E. Koel, and A. A. G. Requicha, *Nat. Mater.* **2**, 229 (2003).
- ²²S. A. Maier, P. G. Kik, and H. A. Atwater, *Phys. Rev. B* **67**, 205402 (2003).
- ²³J. J. Penninkhof, A. Polman, L. A. Sweatlock, S. A. Maier, H. A. Atwater, A. M. Vredenberg, and B. J. Kooi, *Appl. Phys. Lett.* **83**, 4137 (2003).
- ²⁴M. Kaempfe, H. Graener, A. Kiesow, and A. Heilmann, *Appl. Phys. Lett.* **79**, 1876 (2001).
- ²⁵R. A. McMillan, C. D. Paavola, J. Howard, S. L. Chan, N. J. Zaluzec, and J. D. Trent, *Nat. Mater.* **1**, 247 (2002).
- ²⁶H. Mertens and A. Polman (unpublished).
- ²⁷J. J. Penninkhof, T. van Dillen, C. Graf, A. van Blaaderen, A. M. Vredenberg, and A. Polman (unpublished).
- ²⁸M. Quinten and U. Kreibig, *Appl. Opt.* **32**, 6173 (1993).
- ²⁹J. M. Gérardy and M. Ausloos, *Phys. Rev. B* **26**, 4703 (1982).
- ³⁰Q.-H. Wei, K.-H. Su, S. Durant, and X. Zhang, *Nano Lett.* **4**, 1067 (2004).
- ³¹J. R. Krenn *et al.*, *Phys. Rev. Lett.* **82**, 2590 (1999).
- ³²M. L. Brongersma, J. W. Hartman, and H. A. Atwater, *Phys. Rev. B* **62**, R16356 (2000).
- ³³S. Y. Park and D. Stroud, *Phys. Rev. B* **69**, 125418 (2004).
- ³⁴S. A. Maier, P. G. Kik, and H. A. Atwater, *Appl. Phys. Lett.* **81**, 1714 (2002).
- ³⁵*Maxwell's Equations by Finite Integration Algorithm (MaFIA)*, 4th ed. [Gesellschaft für Computer-Simulationstechnik (CST), Darmstadt, Germany, 2000].
- ³⁶*Handbook of Optical Constants of Solids*, edited by E. D. Palik (Academic, San Diego, 1985).
- ³⁷D. M. Peters, C. Strohhofer, M. L. Brongersma, J. van der Elsken, and A. Polman, *Nucl. Instrum. Methods Phys. Res. B* **168**, 237 (2000).
- ³⁸J. P. Kottmann and O. J. F. Martin, *Opt. Express* **8**, 655 (2001).
- ³⁹P. Nordlander, C. Oubre, E. Prodan, K. Li, and M. I. Stockman, *Nano Lett.* **4**, 899 (2004).
- ⁴⁰T. Atay, J.-H. Song, and A. V. Nurmikko, *Nano Lett.* **4**, 1627 (2004).